Eruptive events in the solar atmosphere: New insights from theory and 3-D numerical modelling

Article *in* Contemporary Physics · July 2008

DOI: 10.1080/00107510802366658

CITATIONS
3

READS
133

1 author:

Ilia Iankov Roussev
National Science Foundation
178 PUBLICATIONS **2,498** CITATIONS

SEE PROFILE

Contemporary Physics
Vol. 49, No. 4, July–August 2008, 237–254

Taylor & Francis
Taylor & Francis Group

Eruptive events in the solar atmosphere: new insights from theory and 3-D numerical modelling

Ilia I. Roussev*

Institute for Astronomy, Honolulu, HI, USA

(*Received 9 June 2008; final version received 24 July 2008*)

Ejections of magnetised plasma from the Sun, commonly known as coronal mass ejections (CMEs), are one of the most stunning manifestations of solar activity. These ejections play a leading role in the Sun–Earth connection, because of their large-scale, energetics and direct impact on the space environment near the Earth. As CMEs evolve in the solar corona and interplanetary space they drive shock waves, which act as powerful accelerators of charged particles in the inner solar system. Some of these particles, known as solar energetic particles (SEPs), can strike our planet, and in doing so they can disrupt satellites and knock out power systems on the ground, among other effects. These particles, along with the intensive X-ray radiation from solar flares, also endanger human life in outer space. That is why it is important for space scientists to understand and predict the ever changing environmental conditions in outer space due to solar eruptive events – the so-called space weather. To enable the development of accurate space weather forecast, in the past three decades solar scientists have been challenged to provide an improved understanding of the physical causes of the CME phenomenon and its numerous effects. This paper summarises the most recent advances from theory and modelling in understanding the origin and evolution of solar eruptive events and related phenomena.

Keywords: Sun: corona; Sun: magnetic fields; Sun: coronal mass ejections (CMEs); MHD; shock waves; acceleration of particles

1. Introduction

The solar atmosphere continues to be one of the richest and most dynamic environments studied in modern astrophysics. Spanning many orders of magnitude in density and temperature, while inextricably linked to the complex system of magnetic fields, the Sun displays a myriad of interesting phenomena from sunspots in the photosphere to coronal mass ejections (CMEs) – the most energetic events in the solar system. Even at its most quiescent, the Sun hurls into space a billion-ton cloud of charged particles from the solar corona on average once every 2 days[1]. The charged particles that are produced during CMEs can strike our planet, and in some cases they can disrupt satellites and knock out power systems on the ground. These particles, along with the intensive X-ray radiation from flares, also endanger human life in outer space. That is why it is important to understand and predict the ever changing environmental conditions in outer space due to solar storms – the so-called space weather.

Coronal mass ejections are one of the most astonishing manifestations of solar activity in which vast amounts of magnetic flux ($\sim 10^{13-15}$ Wb) and solar plasma ($\sim 10^{12-13}$ kg) are ejected from the low corona into interplanetary space (see e.g. [1]). These mass ejections were first discovered in 1973 during the Skylab mission as bright features protruding from the solar limb, and at that time they were called coronal transients. During later space missions, such as SoHO (Solar and Heliospheric Observatory), TRACE (Transition Region Analyser and Coronal Explorer), and most recently STEREO (Solar Terrestrial Relations Observatory), it has been realised that CMEs are not some isolated, transient features seen by a particular instrument, but a full-fledged solar phenomenon spawning a rich variety of other processes on the Sun. Over the past 35 years, the solar community has been very active in understanding the physical causes of CMEs.

For a long time, it was thought that solar flares were the dominant sources of geomagnetic activities [2]. A different paradigm, however, has been put forth by [3] in which CMEs, not flares, have been regarded as the main drivers of non-recurrent geomagnetic storms. Today's view is that CMEs and solar flares are interrelated (see e.g. [4]). The two phenomena have been recognised to be two different manifestations of a single physical process that involves a major restructuring of the coronal magnetic field. Statistical studies of CMEs based on SoHO and TRACE observations have indicated that a large fraction of solar flares ($\geq$20%) are associated with CMEs, and that more than

*Email: iroussev@ifa.hawaii.edu

ISSN 0010-7514 print/ISSN 1366-5812 online

DOI: 10.1080/00107510802366658
http://www.informaworld.com

50% of the CMEs are associated with erupting prominences (see e.g. [1]). At present, the main requirement for CME models dictated by observations is two-fold. First, any physical model developed to explain solar eruptions has to account for the fundamental trigger of the eruption. Second, these models must explain the wide variety of features that form and develop in the eruptive process, such as bright H_α ribbons on the solar disk, rising soft X-ray and H_α loop systems in the corona, among other processes (see e.g. [5]). These features, as revealed by both space- and ground-based solar observations, demonstrate the complex nature of CMEs.

This paper summarises the current state of understanding of the origin and dynamics of CMEs, through theory and modelling. The next section discusses the physical requirements that need to be met by the models in order to agree with the relevant observations of solar eruptive events. Sections 3 and 4 describe in detail the two most common groups of CME models to illustrate the basic physical principles involved: the flux-rope models are presented in Section 3 and the sheared-arcade models in Section 4. The more advanced models are discussed in Section 5. The production of SEPs during CME events, and their modelling, is discussed in Section 6. The concluding remarks and future prospects for CME and SEP modelling are presented in Section 7.

2. CME properties and physical requirements for related models

Generally, CME events exhibit the following main properties that need to be accounted for in the relevant models: (i) three-part structure[2] seen in Thomson scattered white-light images; (ii) rapid acceleration near the Sun with asymptotic speed ranging from 4×10^5 m s^{-1} (slow events) to about 2.5×10^6 m s^{-1} (fast events); (iii) total ejected coronal material of about $10^{12–13}$ kg; (iv) bulk kinetic energy of $\sim 10^{24–25}$ J; and (v) carried away magnetic flux of the order of $10^{13–14}$ Wb (see e.g. [1]). In addition, since CMEs are known to originate from regions of closed magnetic field, the CME models also have to account for the opening (at least partially) of the coronal magnetic field all the way to infinity. At the same time, the total magnetic energy of the heliosphere[3] should decrease (see e.g. [6]). This requirement, however, faces the limitations of the Aly–Sturrock theorem [7,8], which states that, as the magnetic field opens up in space during a CME, the total magnetic energy of the system must increase. This, apparently, does not make CMEs possible from an energy stand point. In order to overcome this constraint of the theorem, which applies only to simply connected magnetic field lines, it is necessary for the erupting field configuration to possess knotted field lines (i.e. to have magnetic null points) and/or disconnected field lines (i.e. field lines that are not attached to the Sun). The constraint may also be mitigated if there is a non-ideal magnetohydrodynamic (MHD) process at work, such as magnetic reconnection[4]. Note that magnetic reconnection can reconfigure the coronal magnetic field in the course of the eruption so that the CME becomes energetically possible.

Magnetic observations taken during CME events show that the photospheric magnetic field sources remain virtually unchanged (see e.g. [4]). Hence, in the relevant numerical models, a boundary condition should fix the normal component of the magnetic field at the Sun. This observational constraint implies that the photospheric magnetic sources are unlikely to play a role in energising solar eruptions. Furthermore, it indicates that any coronal disturbance produced by the CME has practically no effect on the massive photosphere because of the enormous difference in mass density ($\sim 10^9$ times) between the photosphere and the corona. In other words, the photospheric footprints of the coronal magnetic field are not affected by the eruption itself on its characteristic time-scale (some tens of minutes). This physical effect is referred to as 'inertial line-tying' of the field.

Another important result revealed from CME observations is the fact that the photospheric magnetic field is driven quasi-statically during the eruption process. The typical value of photospheric motions inferred from observations is of the order of a few thousand m s^{-1} (see e.g. [9]), which is only 0.1–1% of the Alfvén speed[5] in the corona. Thus, if one assumes that magnetic stresses are continuously built in the corona at this characteristic speed, then it would take a few days to store sufficient energy to power a large CME (with energy of $\sim 10^{25}$ J) (see e.g. [4]).

It is important to note here that the solar corona is magnetically dominated, which is characterised by the plasma-β parameter[6]; i.e. $\beta \ll 1$ for the physical environment of the corona. As a result of this, electric currents, $\boldsymbol{J}$, producing the excess magnetic energy from the potential (i.e. current-free) limit must be either force-free (vanishing Lorentz force: $\boldsymbol{J} \times \boldsymbol{B} = 0$, where $\boldsymbol{B}$ is the magnetic field), i.e. field-aligned[7] ($\boldsymbol{J} \parallel \boldsymbol{B}$), or confined to thin current sheets in which $\beta \sim 1$. It has been shown that current sheets are important for producing small compact flares on the Sun when magnetic reconnection sets in and dissipates the sheet (see e.g. [4]). Solar flares have also been thought to be responsible for the production of some of the observed SEPs near the Earth (see e.g. [10]); these SEP events are called 'impulsive' because of the impulsive nature of solar flares. It has been argued, however, that compact

flares cannot explain the ejections of mass and magnetic flux observed during CMEs (see e.g. [5]).

The fact that the high-β current sheets in the corona are unlikely to produce CMEs implies that the energy required for mass ejections to occur is most likely stored in the non-potential magnetic field generated by volumetric, field-aligned coronal currents (associated with low-β regions in the corona). It should be noted here that in solar prominences not all volumetric currents are force-free. This is because some finite Lorentz forces (due to cross-field currents) are required to offset the pressure gradient and gravity forces associated with the presence of cold and dense prominence material (see e.g. [11,12]). It has been demonstrated that these cross-field currents increase the magnetic energy available for a CME launch by not more than 10% above the corresponding force-free portion [4]. Therefore, the presence of cross-field electric currents is not essential for the energy budget of CMEs. These currents, however, could play a role in the CME triggering process if, for example, a large portion of the prominence material ($<90\%$) has been drained by some buoyant instability [11], which results in an imbalanced Lorentz force pointing away from the Sun; this force acts to accelerate the remaining prominence mass and embedded magnetic field outwards.

It is evident from the discussion so far that the energy required to power a coronal mass ejection is most likely stored in the non-potential magnetic field of volumetric coronal currents. It was demonstrated by [9] that among all the forms of energy in the corona only the non-potential magnetic field has the required energy density (~ 10 J m^{-3}) to explain the energetics of CME events. For example, if one imagines a cube of coronal volume with a linear size[8] of 2×10^8 m, and assumes that this volume is filled with magnetic field with a typical field strength of $\sim 3.0 \times 10^{-3}$ T, then a decrease in the field strength by only 20% (i.e. net change of 6.0×10^{-4} T) is sufficient to energise a CME with bulk kinetic energy of 10^{25} J.

2.1. Types of CME models

The physical mechanisms of CME initiation are the subject of active research and debate [4,11]. The discussion so far favours the so-called 'storage' models of solar eruptions, which are well established in the community (see e.g. [4]). Other types of models, for instance the 'flux injection' model of [13], will not be addressed here because of their limited applicability. The basic principle behind the 'storage' models is that magnetic stresses (i.e. volumetric electric currents) are continuously built in the coronal volume by the omnipresence of magnetic flux emergence and shuffling of footprints of coronal loops due to convective motions, among other processes. The slow but steady energy build-up in the corona proceeds up to a point where the mechanical equilibrium of the coronal magnetic field is no longer attainable and, as a result, a CME occurs. The eruption process releases some of the excess energy stored in the non-potential magnetic field – the one associated with volumetric, field-aligned coronal currents.

The majority of existing 'storage' models can be organised into two main groups depending on the assumed state of the coronal magnetic field prior to the eruption. The first class of models (see e.g. [12,14–19]) assumes that a magnetic flux rope (see Section 3 below) exists prior to the eruption. The rope is suspended in the solar corona by a balance between magnetic compression, hoop, and tension forces associated with the magnetic field of the rope and the background field. Both theoretical and numerical studies of magnetic flux ropes suggest that they may suddenly lose mechanical equilibrium and erupt due to foot-point motions, or injection of magnetic helicity[9] at the photosphere. The second group of models (see e.g. [20–26]) relies on the existence of sheared magnetic arcades (see Section 4 below), which become unstable and erupt once a critical state is reached in the corona. In this case, a flux rope does not exist prior to the eruption, but is created as the coronal magnetic field reforms during the eruption process due to magnetic reconnection. To date, there is no convincing observational evidence that proves or disproves either class of models, and no model is advanced enough to explain real events.

It is worth mentioning here that in the pioneering numerical studies of CMEs, the eruptions have been modelled by the injection of dense plasma through some inner boundary placed upstream of the critical point of the solar wind (typically at $R > 20\ R_\odot$) (see e.g. [27]). These earlier models have provided physical insight into how a large solar disturbance travels and interacts with the large-scale solar wind. However, they have relied on *ad hoc* inputs to the solar wind, while ignoring a self-consistent CME initiation scenario, as in the flux-rope and sheared-arcade models. Only recently has the evolution of a CME from the inner corona to 1 AU[10] (and beyond) been numerically modelled in two-dimensional (2-D) (see e.g. [28–30]) and three-dimensional (3-D) (see e.g. [31,32]) settings. The time-dependent magnetic structure of over-expanding CMEs in the solar wind and the dynamic forces acting on them as they evolve in the heliosphere have also been studied at length (see e.g. [33–35]). Although idealised, these numerical studies have reproduced many generic features of CMEs seen in relevant observations.

3. Flux-rope models

The basic topology in the flux-rope models is a twisted rope of magnetic field (i.e. inter-wound field lines) suspended in the solar corona by a balance between magnetic compression, hoop, and tension forces associated with the magnetic field of the rope and the ambient field. The majority of flux-rope models do not discuss the means by which the flux rope has formed in the corona prior to the eruption. Instead, these models focus on exploring the stability properties of flux ropes in the context of CME generation. Some models argue, however, that the rope has emerged from the solar convection zone as a coherent magnetic structure (see e.g. [11]). Recent numerical simulations [36,37] have demonstrated the emergence of a twisted magnetic flux tube from below the photosphere into a pre-existing coronal magnetic field. These studies have predicted solar features and dynamics that are generally consistent with observations.

Assuming the background coronal field to be a superposition of a dipole field plus the field of a line-current, I_0, [17] have demonstrated that the equilibrium of an axially symmetric flux rope with total electric current I has two possible equilibrium positions, provided that the current I is not too large. This configuration[11] is shown in Figure 1. The equilibrium loop location closest to the Sun is stable, whereas the one farthest from the Sun is unstable. As the current I of the flux rope is increased, the two equilibrium locations approach one another, and they meet when the current reaches a critical value, I_{cr}. No stable equilibrium exists for ropes with $I > I_{cr}$ [17]. The difference in the stability properties of the two equilibrium locations comes from the fact that one sits in a magnetic energy valley, whereas the other one sits on a hill. In other words, for the stable (unstable) equilibrium, a small outward displacement of the flux rope leads to an inward (outward) force, which acts to decrease (further increase) the displacement. Alternatively, for flux ropes with fixed current I, the mechanical balance of the rope with the surrounding field can be disrupted if the photospheric sources of the ambient field are either reduced below a critical point (see e.g. [38]), or are moved closer to one another without reduction of the photospheric field (see e.g. [16]). A loss of equilibrium could also occur due to the emergence of new magnetic flux on the Sun (see e.g. [26]).

When the system comprising the flux rope and the background magnetic field is brought to a critical point where a stable equilibrium no longer exists, the growth of MHD perturbations leads to an ideal instability either toroidal (see e.g. [18,39]), or kink-like (see e.g. [40,41]), and a vertical current sheet forms (see e.g. [42]). The electric current in the vertical sheet is always of the same sign as the flux rope current, hence the sheet attracts the current loop. As a result, the erupting flux rope cannot escape, unless a non-ideal process, such as magnetic reconnection, dissipates the current sheet fast enough. (Note that the reconnection process manifests itself as a solar flare.) If the current does not dissipate fast enough [18], then the erupting flux rope is doomed to fail and no CME occurs, only a flare. There

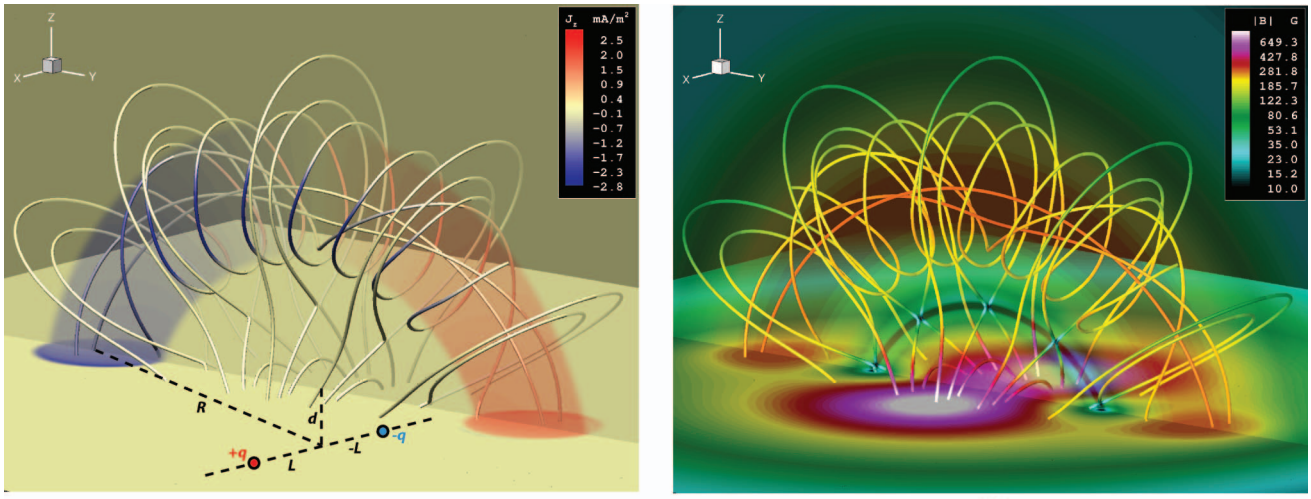

Figure 1. (*a*) Three-dimensional view of the flux rope configuration of [17] with the line-current, I_0, removed. The solid lines are magnetic field lines and the false colour visualises the vertical component of the current density, J_z, in mA m^{-2}. The geometry of the sub-photospheric charges, $+q$ and $-q$, is also shown. (*b*) Same configuration as on the left panel, but now the false colour illustrates the strength of the magnetic field, $|\boldsymbol{B}|$, in Gauss ($= 10^{-4}$ T).

are numerous examples of failed eruptions on the Sun to support this conjecture, for instance the event observed by TRACE on 27 May 2002 in association with a M2-class flare [43].

Below we discuss in detail the analytical flux-rope model of [17] (T&D hereafter), which has been proposed to explain the occurrence of flares and CMEs. The T&D model uses a fully 3-D magnetic field geometry, which looks remarkably realistic when compared with observations. Inspired by this model, [18,40,41] have carried out 3-D MHD numerical studies to test the model in the context of CME generation. Previous 2-D flux-rope models (see e.g. [16]) have suggested than a CME would occur provided that the anchoring of the ends of the flux rope to the Sun does not prevent it, as argued by [20].

The T&D model consists of a circular flux rope with total current I and major radius R, which is embedded in a line-tying surface, as shown in Figure 1. The hoop force of the rope [39], $F_{\text{hoop}} \sim I^2/R$, is counterbalanced by the Ampére force, $F_{\text{Amp}} \sim IqL/(L^2 + R^2)^{3/2}$, acting on the rope current by the outer dipole field from two point magnetic charges, $+q$ and $-q$. The two charges are buried at a depth d below the surface, and they are separated along the x-axis by $\Delta x = 2L$. In addition to the external field generated by the point charges, the T&D model also allows a contribution from an infinitely long line-current, I_0, which flows from $+q$ to $-q$ along the line connecting the two charges. The role of the toroidal field produced by this imaginary, sub-photospheric line-current is to reduce the field-line pitch within and outside the flux rope. Without the line-current, the field lines at the 'surface' of the flux rope are purely poloidal, and they have an infinite number of turns in a finite length, as shown in Figure 1. Some solar observations (see e.g. [44]), however, indicate that the maximum number of turns is less than two, but these observations do not include the dark cavity region, which may comprise most of the flux rope volume. Incorporating the line-current, I_0, eliminates this problem by creating a toroidal field inside the flux rope, thus ensuring that no field line is highly twisted. By adjusting the strength of the line-current, one can achieve a reasonable amount of twist everywhere.

The stability of the T&D configuration has been examined in [17], and it has been found that the rope may become unstable if the large radius, R, exceeds $2^{1/2}\,L$. This is, however, only a necessary condition for the toroidal instability [39] to occur, because the analysis of [17] has not included the effects of the line-tying of the poloidal field circulating around the flux rope. Indeed, the numerical study of [18] has demonstrated that this condition is not a sufficient one, and that larger values of R in excess of 5 L are required to achieve an eruption. They have also found that even when the initial equilibrium is unstable, the flux rope cannot escape, unless the static arcade field associated with I_0 has been removed. Thus, although the T&D model can produce a CME-like eruption, it cannot do so without requiring a highly twisted field at the surface of the flux rope, as illustrated in Figure 1. It may be possible in the future to mitigate this by using a configuration in which the infinitely long line-current, I_0, is replaced by a current loop encircling the Sun whose magnetic field falls off more rapidly (i.e. quadratically) with height.

If the line-current I_0 is present in the magnetic configuration, as in the numerical studies of [40,41], then the T&D configuration has been found to be unstable with respect to the ideal kink-mode instability[12]. The two studies have found that the threshold for instability increases as the major radius of the rope, R (as well as aspect ratio of the rope) becomes larger. The growth of kink perturbations is eventually slowed down by the surrounding potential field produced by the line-current. In agreement with the results of [18], a global CME-like eruption is not plausible unless I_0 is removed. Once the eruption starts and the flux rope begins to lift off, a vertical current sheet forms beneath the rope, which acts to decelerate it. In other words, the symbiosis between the flux rope current and the sheet current may inhibit a successful CME. Then, the sudden onset of magnetic reconnection plays a crucial role in dissipating the current sheet, thus helping the flux rope escape. The dissipation of the current sheet manifests a two-ribbon flare. It is also important to mention here that in the 3-D case, the torsional Alfvén waves play an important role in the eruption process since they transport helicity (or twist) from the footprints of the flux rope to its top. This process acts to sustain the eruption. The effect of the line-tying at the ends of the rope, however, act to decelerate it, as predicted by [20]. In future investigations of the T&D model, or similar models, a more realistic treatment of the reconnection process in the current sheet and the incorporation of a spherical geometry may greatly reduce the deceleration that has been observed in the simulations of [18]. For the first time, these simulations have demonstrated that a fully 3-D line-tied flux rope can lose equilibrium and erupt, at least in principle, and that the anchoring of the flux rope does not automatically prevent an eruption.

There is also a sub-class of flux rope models, which include the presence of prominence material (see e.g. [12]). As discussed earlier on, to ensure stable equilibrium these models require the existence of some non-vanishing Lorentz forces[13] to offset the weight of the prominence; in other words, these are non-force-free-field models. A CME in this case can

be achieved via some buoyant instability mechanism (see e.g. [11]) in which most of the prominence mass (as much as 90%) has been drained through the footprints of the flux rope. An example is the analytical model of [12] (G&L hereafter), which has a complex magnetic topology of a spheromak[14]-type flux rope distorted into a 3-D teardrop shape. The rope itself possesses sufficient free energy needed for an eruption to occur. In a series of numerical studies, [45,46] have investigated the dynamics of the eruption predicted from the G&L analytical model. In these 3-D simulations, the G&L flux rope was superimposed onto a global MHD solution of the solar corona (with bi-modal solar wind), and it was embedded in a helmet steamer[15] at the equatorial region of the Sun. The MHD simulations have shown that by removing 20% of the prominence mass, the resulting eruption yields the observed values for ejected mass ($\sim 1.0 \times 10^{12}$ kg) and kinetic energy ($\sim 4.0 \times 10^{24}$ J) during typical CMEs. The fast ejection (with speed in excess of $\sim 1.0 \times 10^{6}$ m s^{-1} near the Sun) drives a shock wave and interacts with a structured, bi-modal solar wind. The modelled CME has been found to propagate faster in the fast background wind than in the region occupied by the slow wind. As a result, a 'dimple' is formed at the leading edge of the ejection. Manchester et al. [46] have reported on the presence of post-shock compression due to the deflection of magnetic field lines. They have also found a magnetic field enhancement on the back side of the CME, which creates a region of reverse shock compression. It has been argued that these two effects have important implications for the diffusive acceleration of solar particles by the interplanetary CME. In these simulations, the CME has been propagated out to 1 AU, and it has been shown that the interplanetary transient arrives at the Earth with geoeffective properties. Thus, Manchester et al. [46] have demonstrated how an analytical flux-rope model can be incorporated within the framework of a global MHD model of the solar wind to investigate the dynamics of CMEs in interplanetary space, the consequences for the production of SEPs, and the impact of the ejecta on geospace.

4. Sheared-arcade models

The basic topology in this class of models is a magnetic arcade that is subject to shearing motions at the photosphere. As the result of these motions, volumetric electric currents are built along the stressed magnetic field of the arcade, which causes the magnetic energy of the system to increase over time. In this process, the magnetic configuration involving the arcade evolves through a sequence of states close to equilibrium, provided that the magnitude of the photospheric motions is a small fraction (0.1–1%) of the Alfvén speed in the corona. The free magnetic energy (i.e. the energy in excess of the potential limit) in the sheared arcade provides the energy budget for a successful CME once a loss of mechanical equilibrium occurs.

The sheared-arcade models invoke a non-ideal MHD process, i.e. magnetic reconnection, to achieve an abrupt loss of equilibrium of the coronal magnetic field and a subsequent eruption. Unlike the previous class of models, here magnetic reconnection is not a consequence of the eruption process, but the fundamental trigger of the eruption (i.e. responsible for its onset and further development in a run-away fashion). Another main difference is that in the sheared-arcade models a flux rope does not exist prior to the loss of equilibrium (or confinement), but is formed in the course of the eruption. Depending on the height at which the reconnection process occurs in these models, there are three sub-classes, namely: (i) flux-cancellation (see e.g. [21]), (ii) tether-cutting (see e.g. [47]), and (iii) magnetic breakout (see e.g. [20]) models.

In the 'flux-cancellation' models (see e.g. [21,22,25,48,49]), magnetic reconnection takes place at the photosphere, or near the base of the corona. Here a flux rope is formed by reconnecting the opposite polarity feet of a shared magnetic arcade. Once the flux rope starts forming, the dynamics of the eruption proceed in much the same manner as in the flux-rope models. The only difference is that in the flux rope models the total current remains unchanged during the eruption, whereas here the current increases monotonically as the flux rope forms.

In the 'tether-cutting' models (see e.g. [47,50]), a CME is achieved by means of magnetic reconnection inside a prominence (or filament) in the low corona – a process referred to as 'runaway tether-cutting'. The filament here is comprised of a number of magnetic strands and the reconnection process occurs between the threads of opposite polarity that contact each other. The internal reconnection starts at the very beginning of the filament eruption, and it grows in time as the eruption advances. In this process, all connections (tethers) of the filament with the photosphere are broken (cut), except for those at the feet of the erupting flux rope.

In the 'magnetic breakout' model of [20], the eruption is again triggered by magnetic reconnection, but here this process occurs in a curved, horizontal current sheet situated above the magnetic arcade being sheared. In this case, the underlying magnetic geometry is quadrupolar, whereas that in the 'flux-cancellation' models is typically dipolar. A sketch of

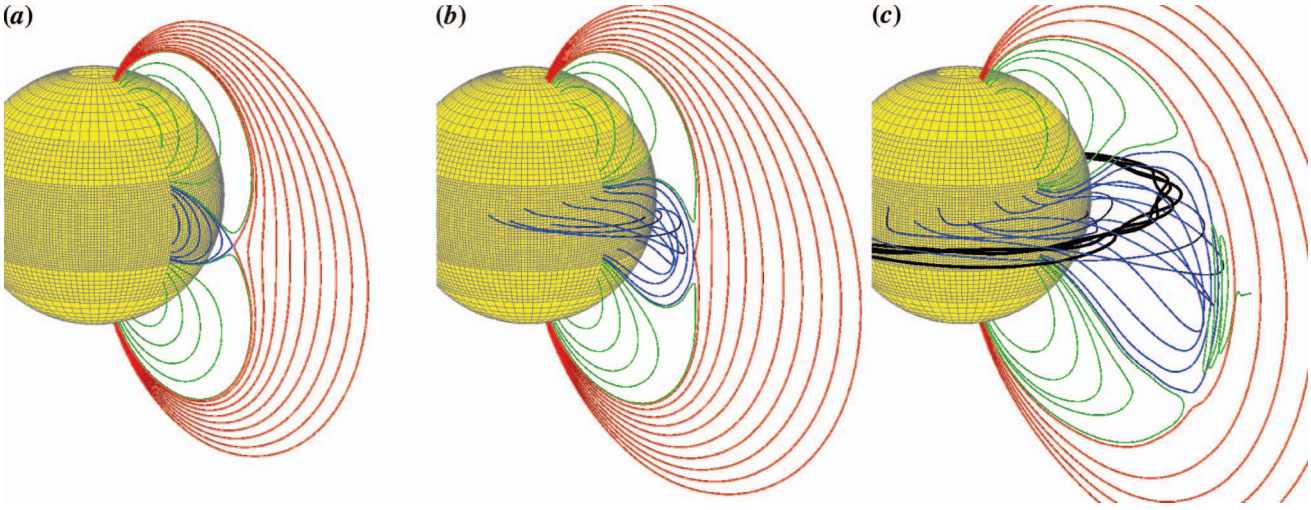

Figure 2. Basic features of the magnetic topology and field-line dynamics in the model of [20]. The different colour lines are magnetic field lines from distinct magnetic flux systems. The initial state is shown in (*a*). As the purple field lines are sheared along the solar equator (*b*), field-aligned volumetric currents are created and the flux system begins to expand. As the result of outward expansion of the sheared-arcade region, a curved, horizontal current sheet is formed between the red and the purple field lines. The sheared field lines begin to erupt (open up) once the unsheared magnetic field from above starts reconnecting in the sheet (*c*). The flux rope formed during the 'magnetic breakout' is visualised as the thick black lines (image templates courtesy of B. Lynch).

the magnetic topology involved in the model, which has a cylindrical symmetry with respect to the Sun's rotation axis, is shown in Figure 2. Because of the axial symmetry, the geometry of the original 'breakout' model was 2.5-D. Very recently, however, there has been a numerical demonstration of the 'breakout' mechanism in a fully 3-D geometry [51]. The 3-D model, however, has failed to produce a successful CME, but rather a confined eruption; that is, a CME that does not escape the Sun, but instead comes to a rest in the outer corona.

The basic physics of the 2.5-D 'breakout' model are as follows. As the central arcade above the equator (shown in purple in Figure 2) is continually sheared, it starts to expand outwards and fills an increasing fraction of the coronal volume. During the expansion, the sheared field lines push against the pre-existing X-line[16] from below. As a result, a curved, horizontal current sheet forms between the purple and the red field lines. This sheet acts to confine the sheared arcade underneath, so that it cannot open in the volume above the sheet. The only way for the sheared arcade to open up is by dissipating the current sheet. Once the reconnection process starts, the field lines above the sheet are moved out of the way of the expanding arcade and the newly formed field lines join the two magnetic flux systems on the side (shown in green). However, rapid reconnection in the sheet does not occur at first. Instead, as the velocity shear increases in the central arcade, the diffuse current transforms into a thin sheet, which then undergoes fast reconnection. The rate of reconnection accelerates as the dissipating current sheet is pushed further away from the Sun. The nature of the transition from slow to fast reconnection has been investigated in detail in the 3-D version of the 'breakout' model [51]. Recalling the 'flux-cancellation' models, there is a series of fully 3-D numerical MHD studies by [21,22,48], and most recently by Amari et al. [25], which demonstrate how a flux rope can be formed by reconnecting the opposite polarity footprints of a sheared magnetic arcade. This mechanism was originally proposed by van Ballegooijen and Martens [52], and it has been simulated for the first time by Inhester et al. [53] in a 2-D geometry. In the 'flux-cancellation' models, continued reconnection of the feet of the arcade weakens the ability of the overlying, unreconnected magnetic field to confine the newly formed flux rope and, eventually, the rope erupts. In MHD simulations with continually evolving boundary conditions, however, some care needs to be taken to determine whether the subsequent evolution is actually due to a true loss of equilibrium, or simply a consequence of some unphysical boundary driving.

4.1. Practical application of 'flux-cancellation' models

The CME models of [21,22,48] have hinted at a practical approach of creating a line-tied flux rope in an arbitrary, 3-D geometry. The schematics are illustrated in Figure 3. As the first step, one needs to apply shear-type horizontal motions along the polarity

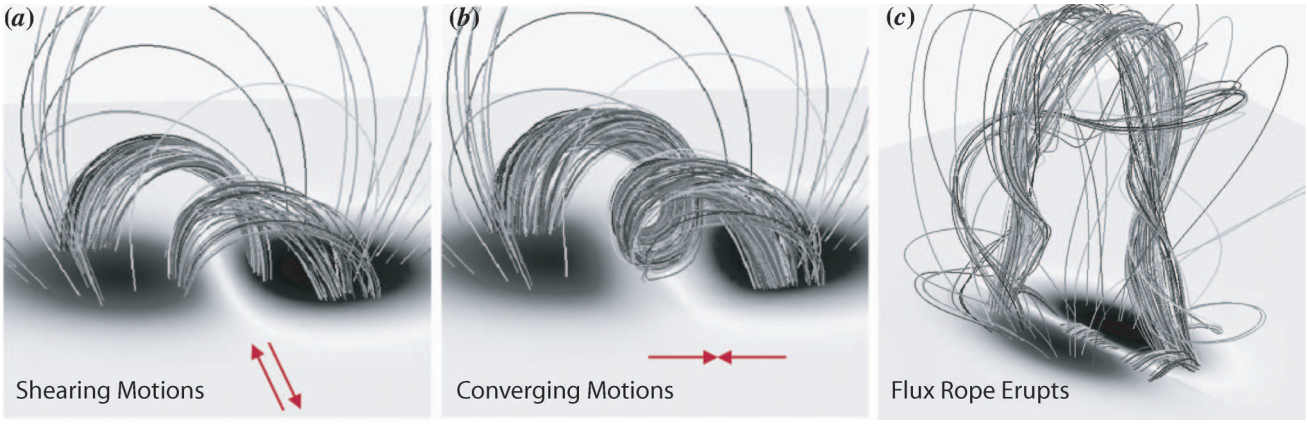

Figure 3. Formation of a 3-D flux rope by flux cancellation and subsequent eruption (after [21,22]). (*a*) The rotation of two magnetic spots acts to shear the magnetic field lines along the PIL and builds field-aligned currents in the corona. Thus, the initially potential magnetic field evolves to a non-potential, force-free field. This is the 'storage' phase in which free energy is monotonically built in the solar corona needed to power a CME. (*b*) The action of converging motions towards the PIL triggers magnetic flux cancellation near the solar surface. This causes the sheared field lines on either side of the PIL to start reconnecting, which leads to the formation of a flux rope. (*c*) The weakening of the overlying field due to flux cancellation, while the flux rope continues to increase in size and strength (or twist), leads to a state of loss of confinement and subsequent eruption.

inversion line (PIL) separating two magnetic spots (see Figure 3(*a*)). These motions can resemble, for instance, the apparent rotation (in the same direction) of the two spots of a magnetic dipole. There are numerous examples from related solar observations supporting the sunspot-rotation scenario (see e.g. [54]). As the magnetic spots rotate and introduce shear along the PIL, the initially potential field evolves through a sequence of states close to equilibrium to a non-potential, (nearly) force-free field. During this 'storage' phase free energy is built in the coronal magnetic field in the form of field-aligned currents. This is the energy that will eventually power the CME. At some later stage, the process of flux cancellation may occur if, for instance, new magnetic flux of opposite polarity begins to emerge in the vicinity of the PIL. This can be modelled by applying converging-type horizontal motions towards the PIL (see Figure 3(*b*)). As illustrated, a flux rope forms as the result of continuing reconnection between the sheared field lines on either side of the PIL. While during the 'storage' phase the distribution of the normal component of the magnetic field, B_R, is preserved, in this second phase B_R changes, i.e. it decreases by absolute value. In essence, this leads to the weakening of the ambient magnetic field confining the newly formed flux rope. This is a run-away process in which the rope at one point can no longer be held in equilibrium with the surrounding field. As a result, the rope erupts, manifesting a CME (see Figure 3(*c*)). It should be noted here that not all of the energy built during the 'storage' phase is released in the eruption process, but only some 8–17% depending on the global magnetic geometry (see e.g. [25]). The released energy is converted into heat and kinetic energy of plasma bulk motions. Some energy is also carried away by the accelerated charged particles during the eruption.

4.1.1. *Case study of 2 May 1998 event*

This practical algorithm has been realised in the work carried out in [25], and it has been applied in the context of the CME that occurred on 2 May 1998 from active region (AR) 8210. Note again that the model requires two processes to work in synergy, namely: (i) sunspot rotation and (ii) flux cancellation in the CME source region due to the emergence of new magnetic flux of opposite polarity. Both of these processes occurred in AR 8210 prior to the solar eruptive event on 2 May. The study has demonstrated the initiation and dynamics of the CME in the solar corona based on a fully 3-D, compressible MHD simulation. The background coronal magnetic field has been reconstructed using the potential field source surface method of [55], with boundary conditions at the photosphere provided by magnetogram data from the Wilcox Solar Observatory (WSO). In the MHD simulation, realistic solar wind conditions have been achieved using the empirical turbulent heating model of [56]. The CME has been modelled by slowly evolving the boundary condition for the horizontal magnetic field at the Sun to account for the rotation of the main sunspot of AR 8210 – the energy 'storage' phase – followed by an episode of flux cancellation.

Although Roussev et al. [25] have not simulated the actual photospheric motions inferred from the high-resolution vector magnetogram data (see e.g. [57]), their model has been generally consistent with the observed magnetic field dynamics, while initiating the CME in a physically plausible manner. That is, one that extracts magnetic energy stored in the corona by evolving the low-resolution WSO data up to a point when a loss of confinement occurs and the CME starts. The model has succeeded in capturing many of the observed features of the 2 May 1998 event and also general properties of CMEs, such as the pre-event structure of the CME source region, interaction of the ejection with the solar wind, shock formation and evolution in the corona, etc.

A view of the modelled CME at $t = 1.1$ h after the initiation is shown in Figure 4. The ejection achieves a maximum speed in excess of 1.0×10^6 m s^{-1}, which is in close agreement with the SoHO/LASCO[17] observations for the event. The CME drives a shock wave and interacts with a highly structured solar wind. The shock wave is found to reach a fast-mode Mach number in excess of 4 and a compression ratio of nearly 3 at a distance of 4 $R_\odot$ from the Sun. The fact that a strong shock can develop so close to the Sun is very important from the perspective of SEP production by a Fermi acceleration process [58], as discussed for this event in [59].

5. Modelling of CMEs originating from complex active regions

5.1. *Limitations of existing 'toy' models*

To date, significant progress has been made in understanding the basic physical processes involved in causing the CME phenomenon. There is a general agreement in the community that CMEs are the result of a catastrophic loss of mechanical equilibrium of solar plasma confined by the coronal magnetic field. The existing theoretical and numerical models differ in the details by which the CME is achieved, and specifically in: (i) the physical driver of the eruption and (ii) precise means of energy storage in the coronal magnetic prior to the CME occurrence. There is, however, no unified CME model developed as of yet, which can explain the majority of solar eruptive events on the Sun and related phenomena.

In a recent study, Ugarte-Urra et al. [60] have found that: (i) seven out of 26 CMEs can be interpreted with the 'magnetic breakout' model of [20]; (ii) 12 events can be explained with other CME models (in dipolar geometries); and (iii) seven events remain unclassifiable. This implies that ~27% of the observed solar eruptive events are more sophisticated than those modelled in idealised magnetic settings. This also proves that it is necessary to study CMEs on a case-by-case basis, as in [25,26], if we are to understand

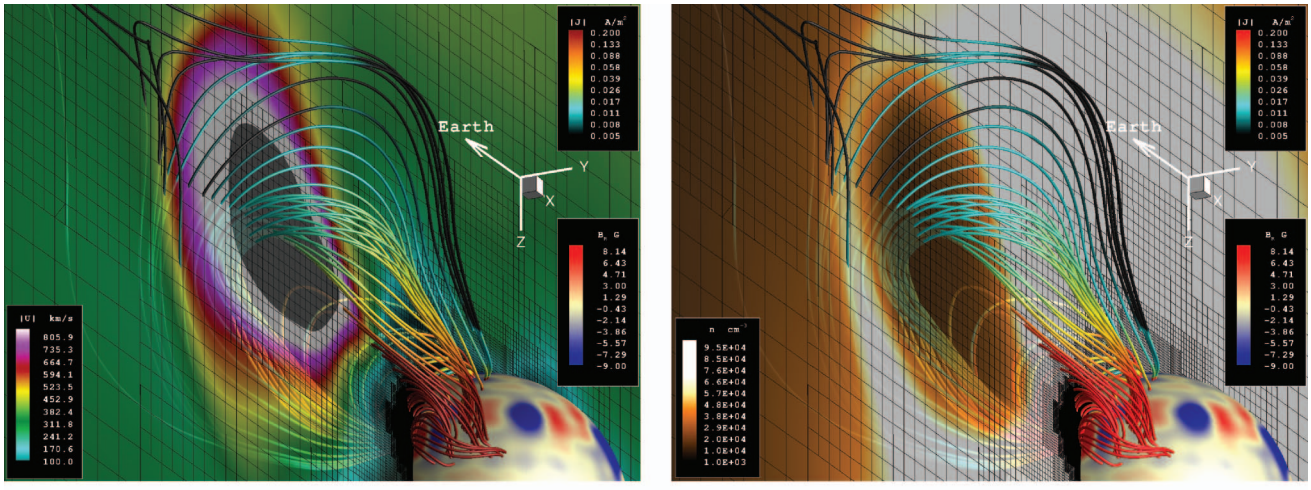

Figure 4. (*a*) 3-D view of the modelled CME on 2 May 1998 at $t = 1.1$ h after the initiation. The solid lines are magnetic field lines and the false colour visualises the magnitude of the current density, $| J |$, in units of A m^{-2} (see colour legend at top right). The magnitude of the flow velocity, $| U |$, in units of km s^{-1}, is shown on a translucent plane (see colour legend to the left). Values in excess of 1.0×10^3 km s^{-1} are blanked and shown in dark grey. The grid-structure on this plane is also shown as the black frame. The inner sphere corresponds to $R = R_\odot$. The colour on the sphere shows the distribution of radial magnetic field, B_R, in units of Gauss (see colour legend at bottom right). (*b*) The same configuration as on the left panel, but now the false colour on the translucent plane illustrates the spatial distribution of the particle density, n, in units of cm^{-3}. The dark cavity region associated with the erupting (and expanding) flux-rope field and the bright leading edge associated with the CME-driven shock wave are clearly seen in the image.

their energetics, dynamics, etc. In a recent study, Roussev et al. [26] have investigated two CME events originating from complex ARs, in particular those that took place on 21 April and 24 August 2002. The next section discusses the magnetic field evolution of the CME source region, and the CME (and related shock wave) dynamics in the low corona.

5.2. *Case studies of 21 April and 24 August 2002 events*

Here we present simulation results for two complex eruptive events, namely the 21 April 2002 CME (CME1 hereafter) and the 24 August 2002 CME (CME2 hereafter), which have been obtained very recently in [26]. The first event, CME1, took place in AR 9906 on the west limb of the Sun. Magnetic field extrapolations in the corona have revealed the presence of large-scale field connections between AR 9906 and ARs 9902 and 9907. That is why CME1 has been regarded as 'CME originating from a complex AR'. The ejection drove a shock wave at a distance of $\sim 1.6 - 1.7\ R_\odot$ (as inferred from SoHO/UVCS observations), which travelled at a speed of $\sim 1.5 \times 10^6$ m s^{-1}; the shock flank arrived at 1 AU in about 51 h. A gradual SEP event also occurred during 21–23 April 2002 in association with the shock dynamics in the interplanetary (IP) space. The observed SEP composition showed a decline in the Fe/C ratio for energies above 10 MeV/nucleon, as reported in [61]. Quite the opposite behaviour (i.e. increase in the Fe/C ratio for energies above 10 MeV/nucleon) was observed for the other event, CME2, despite the fact that both CME1 and CME2 had very similar evolution in the corona. CME2 was similar to CME1 in that: (i) it also occurred on the west limb; (ii) the CME source region, AR 10069, was well connected to a number of nearby ARs (10067, 10068, and 10079); (iii) a shock wave formed relatively close to the Sun and it travelled with a comparable speed (shock flank arrived at 1 AU within 58 h); and (iv) a gradual SEP event occurred on 24–25 August 2002 in association with the eruption. Apparently, CME2 is another event that can be regarded as 'CME originating from a complex AR', which, as discussed below, is even more complex than CME1.

In [61], the observed behaviour of SEP composition for the two events has been attributed to a difference in the shock geometry along the field lines connecting the Sun and the Earth – quasi-perpendicular[18] for CME2 versus quasi-parallel for CME1 – since heavy ions are preferentially accelerated compared to lighter ions at quasi-perpendicular shocks. This hypothesis remains to be investigated, however, which is what has motivated Roussev et al. [26] to model these two events: they appear to be very similar in CME characteristics and so different in SEP properties. Below we compare CME1 and CME2 in terms of the underlying magnetic geometry of the solar corona before and shortly after the CME onset, following [26]. The study comprises fully 3-D compressible MHD simulations of the two events. Since they occurred on the west limb, it is difficult to infer from observations the dynamics of magnetic flux elements on the Sun, which could have led to the ejections. Here, we assume that magnetic flux emergence was the most likely mechanism that triggered the CMEs in both cases[19], and this is what has been modelled.

The initiation model for both CME1 and CME2 resembles one consequence of magnetic flux emergence, namely shearing motions, to achieve loss of mechanical equilibrium and subsequent eruption. In some regard, this model is similar to the 'magnetic breakout' scenario of [20]. In the model, a newly emerged AR is mimicked by the dipolar magnetic field of two point charges, $+q$ and $-q$, which are separated initially (at $t = 0$) by a distance $2L$ and are buried at a depth d below the solar surface, as in the T&D model (see Section 3 above). The model parameters are chosen such that to yield a peak value of the radial magnetic field of the dipole at the solar surface of $\sim 4.7 \times 10^{-3}$ T, which is consistent with observations. The magnetic field produced by the two charges is superimposed into the extrapolated potential magnetic field constrained by the high-resolution SoHO/MDI[20] data. At $t = 0$, the two magnetic charges are moved apart quasi-steadily[21] up to $t = 30$ min (see Figure 1 in [26]). As the result of moving the two charges apart (i.e. flux emergence), the magnetic field lines connecting the two spots of the dipole are stretched and twisted. Thus, the magnetic energy and helicity of the dipole field gradually increase over time, which is what is required to power an eruption. As the coronal field is evolved quasi-steadily, it approaches a state that is no longer stable. Then, as the result of loss of confinement with the overlying field, the 'energised' magnetic field of the dipole erupts. This procedure, although *ad hoc*, enables one to initiate CMEs in realistic coronal magnetic field settings involving the emergence of new magnetic flux. The magnetic field configuration in the case of CME1 at $t = 0$ and $t = 30$ min is shown in Figure 5.

In the shearing process, electric currents are built not only along the stressed magnetic field, but also at the pre-existing null points (NPs) and quasi-separator (QS) (in the case of CME2) of the magnetic configuration since the pressure balance there is perturbed. The magnetic energy of the evolving dipole monotonically increases in time and the loops connecting the two moving spots gradually expand. As the sheared

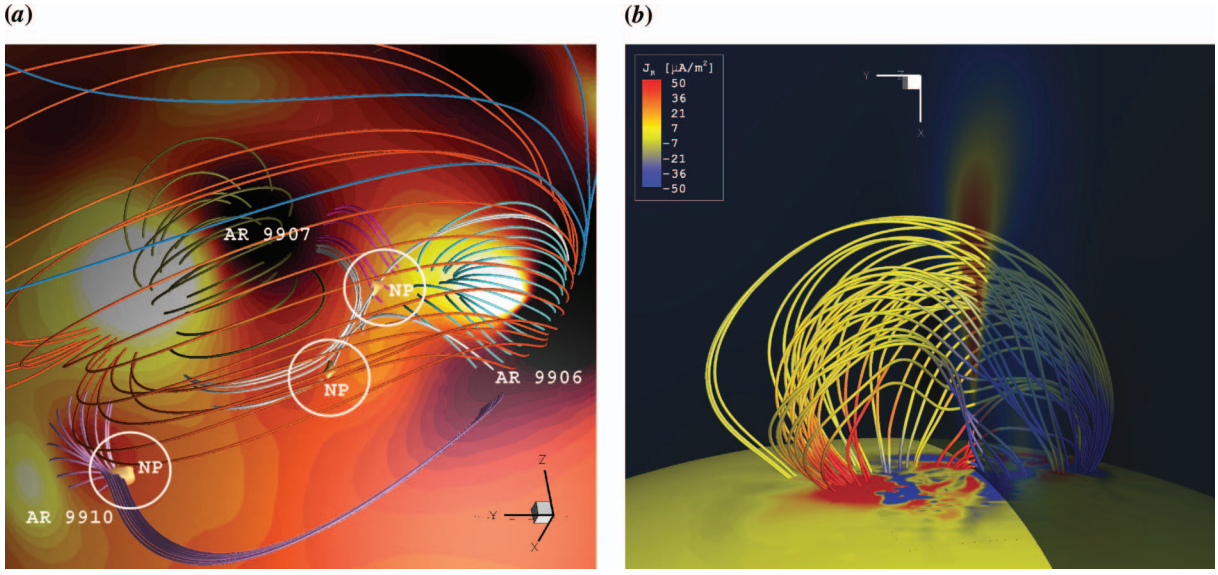

Figure 5. (*a*) Pre-event topology of the coronal magnetic field of relevance to CME1. The ARs of interest are annotated as shown. The coloured lines in the image are 3-D magnetic field lines, where each colour represents a distinct flux system; the dark blue field lines are open in the IP space. The magnetic null points (NPs) in the corona are encircled. The plasma-β has been used as a proxy to visualise the NPs, which are shown as iso-surfaces of $\beta = 0.2$. (*b*) 3-D structure of the erupting magnetic field for the same event. The colour code along the magnetic field lines visualises the radial component of the current density, J_R. The radial velocity of the erupting magnetic field, U_R, is shown on a translucent plane cutting through the middle of the magnetic flux rope; the red (yellow) colour corresponds to a flow speed of $\sim 1.0 \times 10^6$ m s^{-1} ($\sim 7.0 \times 10^5$ m s^{-1}). The solar surface is shown as the yellow sphere (from [26]). Reproduced with permission from Roussev, Lugaz, and Sokolov, Astrophys. J. Lett. 668, L87 (2007). Copyright (2007) by the American Astronomical Society.

field of the dipole expands, it begins to reconnect with the ambient field from the neighbouring flux systems through the pre-existing NPs and QS (in the case of CME2). Due to magnetic reconnection, the overlying magnetic field is removed sideways, as in the 'breakout' model of [20], and thus this field no longer has a restraining effect on the expanding loops from below. Once the 'magnetic breakout' sets in, the free energy stored in the sheared coronal field starts to convert into kinetic energy of bulk plasma motions and heat. In both cases, approximately 3.0×10^{12} kg of solar plasma is ejected from the solar corona into the IP space. The right panel of Figure 5 illustrates the 3-D structure of the erupting magnetic field in the case of CME1.

A very important result from these 3-D MHD simulations is that, because of the inherent complexity of the underlying magnetic field for both events, magnetic reconnection through the nearby NPs located sideways of the expanding field serves to change the connectivity of the erupting field. This results in jump-like changes of the CME footprint(s), which is not a feature of the classical 'breakout' model, or any other CME model with idealised settings for that matter. Other important results are that: (i) the separation between CME footprints increases over time, and (ii) the mutual helicity of the flux systems undergoing reconnection transforms into self-helicity. Also, in the case of CME2, the QS evolves into a large current sheet above the expanding current loop system, which undergoes rapid reconnection as the stressed field from below pushes against it. The fast reconnection in the sheet enables rapid outward acceleration of the current loop. For both events discussed here, the erupting field consists of a mixture of magnetic patches from various flux systems[22]. We argue that the majority of CME events originating from complex ARs undergo similar evolution.

The modelled CMEs in both cases drive shock waves near the Sun, which is in good agreement with observations. A comparison between the simulated structure of CME2 in white light at $t = 48$ min and the corresponding SoHO/LASCO observation is shown in the upper panel of Figure 6. This comparison demonstrates that the adopted models of the background solar corona and CME reproduce rather well the structure seen in white-light observations. The 3-D geometry of CME2 near the Sun and at large distances at $t = 100$ min is shown in the lower panel of Figure 6.

In order to investigate the changes in shock geometry along the IP magnetic field (IMF) connecting the Sun with L1, IMFL1, in the case of CME2 the computational domain has been extended to the Earth's orbit. A time sequence showing the evolution

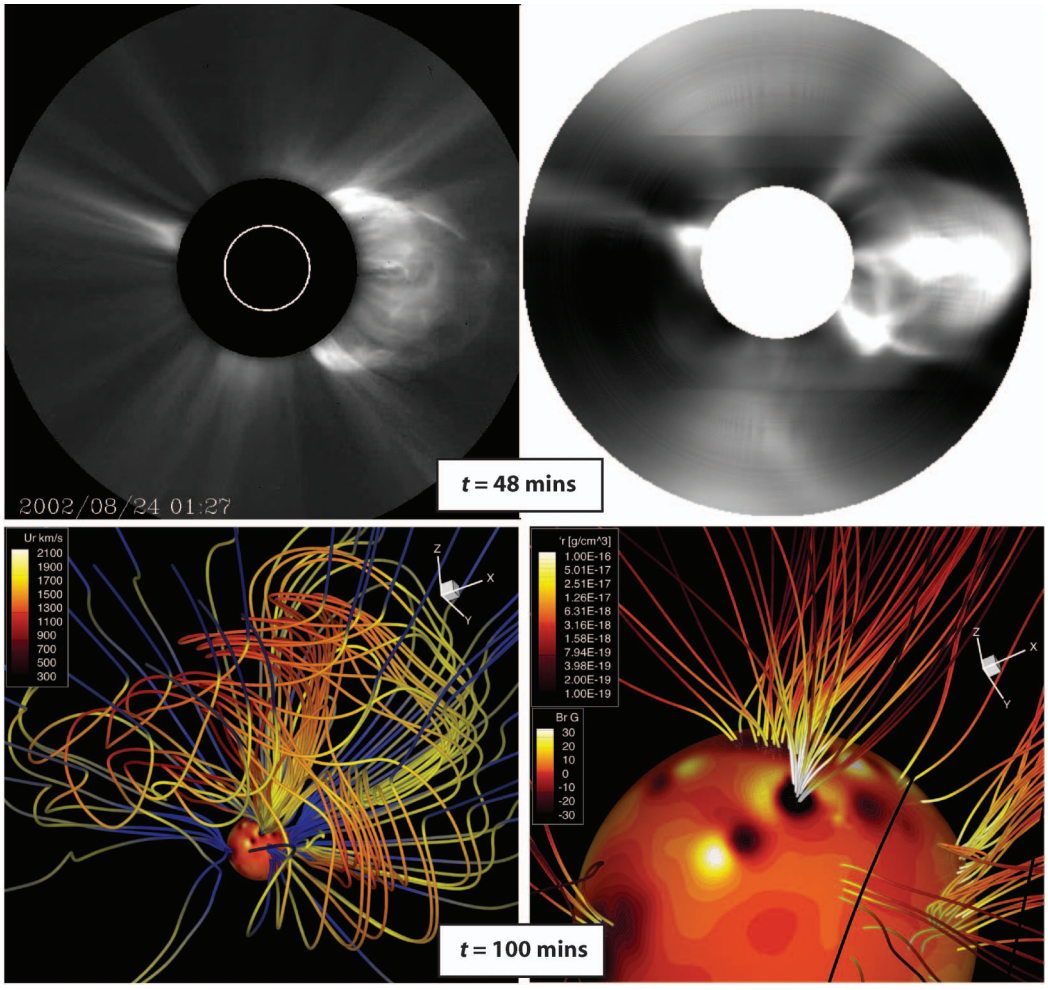

Figure 6. *Upper panels:* SoHO/LASCO observation (at 01:27 UT on 24 August 2002) and simulated structure of the solar corona with CME2 in white light (at $t = 48$ min). *Lower panels:* Simulated 3-D structure of the coronal magnetic field at $t = 100$ min. The colour code at the Sun visualises the radial magnetic field, B_R, in units of Gauss (see lower colour legend on the right image). The coloured lines are 3-D magnetic field lines, where the colour code in the left (right) image illustrates the flow speed, U_R (mass density, ρ) along the lines. The 3-D structure of the CME can be assessed from the left image, whereas the right image illustrates the position of the CME footprints (regions of high mass density, i.e. white areas) at the Sun (image templates courtesy of N. Lugaz).

of the coronal magnetic field passing through the vicinity of L1, with over-plotted velocity flow vectors, is shown in Figure 7. We have found that the shock geometry along IMFL1 changes quite dramatically during the early stages of CME-shock evolution. The shock transforms from quasi-perpendicular to quasi-parallel within $\sim 7\ R_\odot$. Another important result is that the IMFL1 footprint at the Sun changes due to interchange reconnection[23] over the course of the event: the field geometry changes from open to closed and back to open over the course of 45 min. We argue that this process of field connectivity change may enable suprathermal particles produced during the flare to undergo diffusive shock acceleration (see next section) once the closed flare loops become open again. It remains to be investigated whether the same process takes place during CME1.

6. CMEs, solar energetic particles and space weather

There is a consensus in the space science community that CMEs play a leading role in the Sun–Earth connection, because of their large-scale, energetics and direct impact on the space environment near the Earth. As CMEs evolve in the solar corona and interplanetary space they drive shock waves, which act as powerful accelerators of charged particles in the inner solar system. Some of these SEPs can strike our planet, and in doing so they can disrupt satellites and knock out power systems on the ground, among other effects.

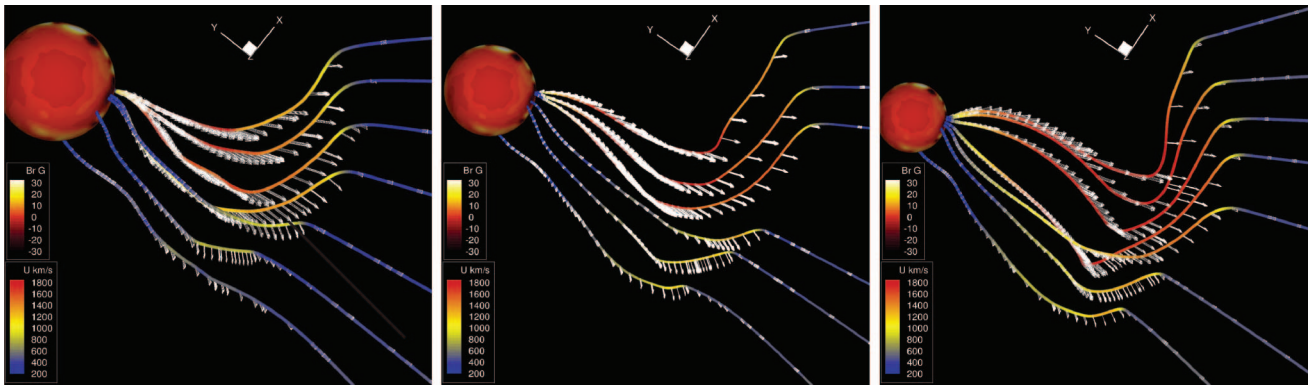

Figure 7. Time-sequence showing the evolution of the coronal magnetic field passing through the vicinity of L1 with overplotted velocity flow vectors. The images on the left, middle, and right correspond to $t = 45$, 60, and 75 min, respectively. The colour code at the Sun visualises B_R (see upper colour legend). The coloured lines are 3-D magnetic lines, where the colour code represents the flow speed along the lines (image templates courtesy of N. Lugaz).

These particles, along with the intensive X-ray radiation from solar flares, also endanger human life in outer space. That is why it is important for space scientists to understand and predict the ever changing environmental conditions in outer space due to solar eruptive events – the so-called space weather.

High-energy solar protons (>100 MeV: 1 MeV $\approx 1.6 \times 10^{-13}$ J) can be accelerated within a short period of time ($\leq$1 h) after the initiation of a CME, which makes them difficult to predict and poses a serious concern for the design and operation of both manned and unmanned space missions. Recent theories (see e.g. [62–66]) and related observations

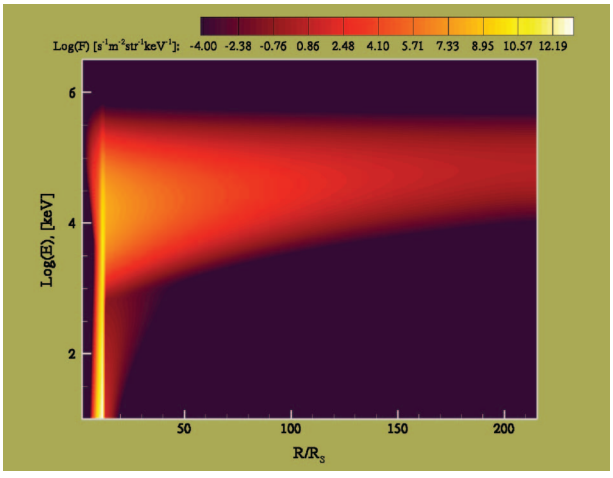

Figure 8. Snapshot of the differential proton intensity as a function of radial distance from the Sun, R, and particle energy, E, at $t = 1.6$ h after the shock wave forms. The shock is located at $R = 12.2R_\odot$ at this time (from [59]). Reproduced with permission from Sokolov et al., Astrophys. J. Lett. 616, L171 (2004). Copyright (2004) by the American Astronomical Society.

(see e.g. [61,67–69]), have suggested that these high-energy particles are the result of Fermi acceleration processes [58] at a shock wave driven by a solar eruption, the so-called diffusive shock acceleration (DSA), in the Sun's proximity (at distances of $2-15$ $R_\odot$). These theories have been debated in the community (see e.g. [10,70,71]) since very little is known from observations about the dynamical properties of CME-driven shock waves in the inner corona soon after the onset of the eruption. The main argument against the shock origin is that near the Sun the ambient Alfvén speed is so large, due to the strong magnetic fields there, that a strong shock wave is difficult to expect [72]. How soon after the onset of a CME the shock wave forms, and how it evolves in time depends largely on how this shock wave is driven by the erupting coronal magnetic field. It has been argued in [61] that the shock geometry plays a significant role in the spectral and compositional variability of SEPs above $\sim$30 MeV/nucleon. This remains to be proven, however, which is why realistic global simulations of CMEs [25,26] coupled to the production of SEPs [59] are very important. In order to explain the observed signatures of gradual SEP events, the global CME models are required to explain the time-dependent changes in the strength and geometry (quasi-parallel versus quasi-perpendicular) of shocks during those events, as discussed in Section 5.2 above.

To address the issue of shock origin during CMEs requires that real magnetic data are incorporated into the global MHD models of the solar corona, as in [56,73]. Recently, Sokolov et al. [59] have carried out a numerical investigation in which they have studied the DSA of solar particles at the realistically driven shock wave in the CME simulation of [25]. For the CME being studied on 2 May 1998, there has been a prompt solar energetic proton event

associated with it and observed by the NOAA[24] GOES-8 satellite.

The SEP study of [59] has shown that the theory of DSA alone can account for the production of GeV protons during solar eruptions, provided that a sufficiently strong shock wave forms near the Sun, as demonstrated in the related CME study. This numerical calculation has been the first of a kind which has accomplished a realistic coupling of a global CME model with a SEP model. Previous related studies have employed either an idealised, spherically symmetric shock wave (see e.g. [66,74]), or that taken from a snapshot of a CME simulation (see e.g. [75]) and extended in time assuming self-similarity of the flow. In turn, Sokolov et al. [59] have taken a different approach in which the production of energetic solar protons has been modelled by following the time-dependent, 3-D evolution of a realistically driven shock wave. For this purpose, they have performed frequent dynamical coupling between a MHD code, BATS-R-US (see e.g. [31]), and a newly developed kinetic code, FLAMPA, to capture time-scales and spatial gradients of dynamical importance for the DSA of solar protons.

Figure 8 demonstrates key features predicted from the theory of DSA, namely: (i) the existence of an 'exponential tail' of particles upstream of the shock wave (length of the tail $\approx D/U_{\rm sh}$, where D is the scalar diffusion coefficient and $U_{\rm sh}$ is the shock speed); (ii) the elevated proton intensities at high energies behind the shock wave; and (iii) the escape of high-energy (>10 MeV) particles upstream of the shock wave. The latter is due to the fact that $D \propto E$ (where E is the kinetic energy of particles), meaning that once the particles are accelerated to high energies their upstream tail becomes very large. These are the particles of particular importance for space weather, because they are considered as precursors of disruptive events in the space environment near the Earth.

The results of the coupled CME-SEP simulation of [59] have clearly demonstrated the capability to provide a high-performance simulation of the acceleration and transport of solar protons observed early during gradual SEP events. There are, however, some discrepancies between the observed proton fluxes by GOES-8 on 2 May 1998, and those obtained from the model. Also, the onset of the observed SEP event had occurred $\sim$30–60 min after the onset of the flare, whereas in the coupled simulation this has been achieved $\sim$30 min after the shock wave formed (or $\sim$60 min after the onset of the eruption). This implies that it is important to derive from the CME model when, or if, a shock wave forms on the magnetic field line connecting the Sun with the Earth (or the first Lagrangian point, L1). Furthermore, this also shows that a coupled model is very informative and allows one to use real SEP data to verify it.

The kinetic code used by Sokolov et al. [59] is a relatively new tool that incorporates many essential features of the theory of shock acceleration and transport of solar particles. Further extensions of this code, however, are necessary in order to address the wide range of SEP variability, which is a key issue for developing a predictive capability for SEPs. One example of such extensions is the role of self-generated Alfvén waves, which have been demonstrated to have important consequences for SEP elemental abundance variations (see e.g. [63,69]) and the evolution of SEP anisotropies (see e.g. [76]). Another example is the possible role of the shock geometry in controlling the spectral shapes of the highest energy SEPs [61] and the energy injection threshold (see e.g. [77,78]). Extensions such as these are very important for understanding the observed variability during gradual SEP events and should be present in the relevant numerical models.

7. Conclusions and future prospects for CME models

The models proposed to date agree in describing the general properties of CMEs, although the vast majority of them involve idealised magnetic settings (either bipolar or quadrupolar). In the study by Ugarte-Urra et al. [60], it has been found that $\sim$27% of the observed events, like CME1 and CME2 discussed above, are more sophisticated than those modelled in idealised configurations. This shows that the existing models are not sufficiently well developed to explain the real solar events; this also proves that it is necessary to study CMEs on a case-by-case basis, as done in [25,26], in order to understand their dynamics, energetics, and IP consequences.

At present, the two competing groups of CME models are the flux-rope and the sheared-arcade models. These two classes of so-called 'storage' models differ on two major points. First, in the flux-rope models, it is assumed that a flux tube comprising a region in the corona of strong concentration of volumetric electric currents exists *prior* to the eruption. In the sheared-arcade models, in turn, the flux rope forms *during* the eruption. Second, while both classes of models invoke a non-ideal MHD process to explain CMEs, in the flux-rope models magnetic reconnection is a *consequence* of the eruption, while in the other group reconnection is the fundamental *trigger* of the eruption. To date, there is no convincing observational evidence that proves or disproves either class of CME models. The existence of flux ropes prior to CMEs is still unclear. To determine this, one needs precise measurements of the coronal magnetic field, but this

data collection has just started (see e.g. [79]). As for the shear-arcade models, the origin of shear is still a mystery, although the rotation of magnetic sunspots evident from observations is one way to introduce shear along the PILs required in the models.

In the sheared-arcade models, the fundamental trigger of the CME, namely magnetic reconnection, somehow disrupts the force balance of the coronal magnetic field, thus starting the eruption. A delay in the turn-on of the reconnection process, however, is required in order to store sufficient energy in the corona needed for powering the CME. This naturally raises the question about the nature of micro-instabilities in current sheets leading to enhanced, or anomalous, resistivity. The nature of this resistivity is poorly understood, however. To improve the present understanding of this process requires the development of a comprehensive theory of magnetic reconnection in three-dimensions.

Improved understanding of CMEs also requires developing more realistic coronal magnetic field models in which *vector* magnetic field measurements (e.g. those from NSO/SOLIS[25] and future SDO/HMI[26]) are used as boundary conditions. Apart from this, realistic plasma properties[27] at the photosphere and in the solar corona are also needed to drive the models. At present, this is far from being realistic. Future improved solar observations (e.g. those from SDO) are expected to provide a more complete and realistic set of initial and boundary conditions to drive those computational models of CMEs, so that reliable tools for space weather predictions become available to the space science community.

The future prospects for CME modelling are very optimistic primarily because the new NASA STEREO mission (see e.g. [80]) provides an ideal opportunity for CME theorists and modellers to answer some of the outstanding issues raised here. The multi-dimensional solar observations by STEREO/SECCHI help determine the magnetic field geometries that exist prior to solar eruptions, because once CMEs take off the two STEREO spacecraft (A and B), jointly with SoHO, observe the erupting filaments and coronal structures from multiple vantage points. These observations follow the propagation of solar and interplanetary transients all the way from the Sun to the Earth. This is important for testing and validating the numerical models of CME propagation. The future SDO mission, on the other hand, will allow modellers to couple photospheric with coronal magnetic field measurements, and it will enable direct tests for the SEP models. Overall, both the STEREO and SDO missions will provide a new, multi-dimensional level of coupling between numerical models and observations of solar eruptions and associated phenomena. The realistic data-driven modelling of CMEs and related SEP events is just about to become a reality, which will ultimately lead solar scientists to an improved understanding of this magnificent and complex solar phenomenon.

Acknowledgements

The author would like to thank Cooper Downs, Terry Forbes, Tamas Gombosi, Carla Jacobs, Marty Lee, Jing Li, Yang Liu, Noé Lugaz, Ben Lynch, Chip Manchester and Igor Sokolov and for their collaboration on some of the topics discussed in this review. The research work of I.R. at the IfA is supported by the following grants: NSF ATM-0454469 (FDSS), NSF ATM-0631790 (SHINE), NSF ATM-0639335 (CAREER), and NASA NNX07AC13G (LWS).

Notes

1. The frequency of CME occurrence ranges from 2–3 per day to 2–3 per week.
2. This includes the bright compact core, dark cavity region surrounding the core and bright leading edge.
3. The region extending from the solar surface to the outer boundary of the solar system.
4. Magnetic reconnection is a universal process in plasma physics in which magnetic field lines from different magnetic domains are spliced to one another, thus changing their patterns of connectivity with respect to the sources.
5. This is the speed of an Alfvén wave in a plasma, which is a travelling perturbation of the ions and the magnetic field. The wave is dispersionless with a speed of $B/(\mu_0\,\rho)^{1/2}$, where B is the magnetic field strength and ρ is the plasma mass density.
6. This is the ratio of the kinetic gas pressure to the magnetic pressure.
7. Except in solar prominences, which are bright features above the solar limb seen in H_α images.
8. This is a typical length-scale of a CME source region.
9. Magnetic helicity is the extent to which the magnetic field wraps around itself. This is a generalisation of the topological concept of linking number to the differential quantities required to describe the magnetic field.
10. One astronomical unit (AU) is the average distance between the Sun and the Earth, which is 1.496×10^{11} m.
11. The contribution from the infinite line-current, I_0, is not shown here. In [17], this current flows from $+q$ to $-q$ along the line connecting the two magnetic charges.
12. These studies have suggested the kink instability as a mechanism for the onset of solar flares.
13. These forces are associated with the presence of cross-field currents in the prominence channel.
14. Spheromak is a magnetic fusion energy concept in which the plasma is in MHD equilibrium. The magnetic field of the spheromak is largely self-generated through plasma currents, thus leading to a stable, typically toroidal plasma.
15. Helmet streamer is a region in the solar corona where the magnetic field is closed and the field strength is high enough to trap the solar plasma and keep it from escaping. Plasma accumulates in these regions and forms bright, helmet-like structures seen during solar eclipses.

16. The presence of an X-line (where the magnetic field vanishes) is a unique feature of a quadrupolar-type magnetic setting.
17. Large Angle Spectrometric Coronagraph onboard SoHO.
18. For angles between the shock normal and the magnetic field vector that are $>45^{\circ}$.
19. Note that there is convincing evidence from the SoHO/MDI observations about ongoing flux emergence prior to both events (J. Li, private communication, 2008).
20. Michelson Doppler Imager onboard SoHO.
21. Note here that the speed of charge separation is at most 2% of the local Alfvén speed, which results in quasi-steady evolution of the coronal magnetic field.
22. Those involved in the reconnection process.
23. This is magnetic reconnection between a closed and open magnetic field.
24. National Oceanic and Atmospheric Administration.
25. Synoptic Optical Long-term Investigations of the Sun at the National Solar Observatory.
26. Solar Dynamic Observatory (SDO) is a forthcoming NASA space mission.
27. Realistic to the extent to match quantitatively the observed EUV and soft X-ray emission from the solar disc as well as Thomson scattered white light above the solar limb.

Notes on contributor

Ilia I. Roussev obtained his Ph.D. in 2001 from the School of Mathematics and Physics of the Queen's University Belfast, Northern Ireland, based at the Armagh Observatory. In the same year he moved to Ann Arbor, Michigan, and became a postdoctoral researcher at the Department of Atmospheric, Oceanic, and Space Sciences of the University of Michigan. Since then he has been involved in analytical and computational studies of the solar atmosphere, concentrating on processes that couple the photosphere with the overlying corona and solar wind during quiet and magnetically active times on the Sun. In 2006, he began a tenure-track faculty appointment at the Institute for Astronomy in Hawaii.

References

[1] J.T. Gosling, *Coronal mass ejections and magnetic flux ropes in interplanetary space*, AGU Monograph Ser. 58 (1990), pp. 343–364.
[2] M. Dryer, *Coronal transient phenomena*, Space Sci. Rev. 33 (1982), pp. 233–275.
[3] J.T. Gosling, *The solar flare myth*, J. Geophys. Res. 98 (1993), pp. 18,937–18,949.
[4] T.G. Forbes, *A review on the genesis of coronal mass ejections*, J. Geophys. Res. 105 (2000), pp. 23,153–23,166.
[5] E.R. Priest and T.G. Forbes, *The magnetic nature of solar flares*, Astron. Astrophys. Rev. 10 (2002), pp. 313–377.
[6] P.A. Sturrock, P. Kaufman, R.L. Moore, and D.F. Smith, *Energy release in solar flares*, Sol. Phys. 94 (1984), pp. 341–357.
[7] J.J. Aly, *How much energy can be stored in a three-dimensional force-free field?*, Astrophys. J. Lett. 375 (1991), pp. L61–L64.
[8] P.A. Sturrock, *maximum energy of semi-infinite magnetic field configurations*, Astrophys. J. 380 (1991), pp. 655–659.
[9] R.C. Canfield, C.C. Cheng, K.P. Dere, G.A. Dulk, D. McLean, R.D. Robinson, E.J. Schmahl, and S.A. Schoolman, *Radiative energy output of the 5 September 1973 flare*, in *Solar Flares: A Monogram From the Skylab Solar Workshop II*, P.A. Sturrock, ed., Colorado Assoc. Univ. Press, Boulder, Colorado, 1980, pp. 451–469.
[10] D.V. Reames, *Magnetic topology of impulsive and gradual solar energetic particle events*, Astrophys. J. Lett. 571 (2002), pp. L63–L66.
[11] B.C. Low, *Coronal mass ejections, magnetic flux ropes and solar magnetism*, J. Geophys. Res. 106 (2001), pp. 25,141–25,163.
[12] S.E. Gibson and B.C. Low, *A time-dependent three-dimensional magnetohydrodynamic model of the coronal mass ejection*, Astrophys. J. 493 (1998), pp. 460–473.
[13] J. Chen, *Effects of toroidal forces in current loops embedded in a background plasma*, Astrophys. J. 338 (1989), pp. 453–470.
[14] J. Chen, *Theory of prominence eruption and propagation: interplanetary consequences*, J. Geophys. Res. 101 (1996), pp. 27,499–27,520.
[15] T.G. Forbes and P.A. Isenberg, *A catastrophe mechanism for coronal mass ejections*, Astrophys. J. 373 (1991), pp. 294–307.
[16] T.G. Forbes and E.R. Priest, *Photospheric magnetic field evolution and eruptive flares*, Astrophys. J. 446 (1995), pp. 377–389.
[17] V.S. Titov and P. Démoulin, *Basic topology of twisted magnetic configurations in solar flares*, Astron. Astrophys. 351 (1999), pp. 707–720.
[18] I.I. Roussev, T.G. Forbes, T.I. Gombosi, I.V. Sokolov, D.L. DeZeeuw, and J. Birn, *A three-dimensional flux-rope model for coronal mass ejections based on a loss of equilibrium*, Astrophys. J. Lett. 588 (2003), pp. L45–L48.
[19] S.T. Wu, W.P. Guo, D.J. Michels, and L.F. Burlaga, *MHD description of the dynamical relationships between a flux rope, streamer, coronal mass ejection and magnetic cloud: an analysis of the January 1997 Sun–Earth connection event*, J. Geophys. Res. 104 (1999), pp. 14,789–14,802.
[20] S.K. Antiochos, C.R. Devore, and J.A. Klimchuk, *A model for solar coronal mass ejections*, Astrophys. J. 510 (1999), pp. 485–493.
[21] T. Amari, J.F. Luciani, Z. Mikic, and J. Linker, *Three-dimensional solutions of magnetohydrodynamic equations for prominence magnetic support: twisted magnetic flux rope*, Astrophys. J. Lett. 518 (1999), pp. L57–L60.
[22] T. Amari, J.F. Luciani, Z. Mikic, and J. Linker, *A twisted flux rope model for coronal mass ejections and two-ribbon flares*, Astrophys. J. Lett. 529 (2000), pp. L49–L52.
[23] J.A. Linker and Z. Mikić, *Disruption of a helmet streamer by photospheric shear*, Astrophys. J. Lett. 438 (1995), pp. L45–L48.
[24] W.B. Manchester IV, *Buoyant disruption of magnetic arcades with self-induced shearing*, J. Geophys. Res. 108 (2003), p. 1162.
[25] I.I. Roussev, I.V. Sokolov, T.G. Forbes, T.I. Gombosi, M.A. Lee, and J.I. Sakai, *A numerical model of a coronal mass ejection: shock development with implications for the acceleration of GeV protons*, Astrophys. J. Lett. 605 (2004), pp. L73–L76.

[26] I.I. Roussev, N. Lugaz, and I.V. Sokolov, *New physical insight on the changes in magnetic topology during coronal mass ejections: case studies for the Apr 21 and Aug 24, 2002 events*, Astrophys. J. Lett. 668 (2007), pp. L87–L90.
[27] D. Odstrčil and V.J. Pizzo, *Three-dimensional propagation of coronal mass ejections in a structured solar wind flow 2. CME launched adjacent to the streamer belt*, J. Geophys. Res. 104 (1999), pp. 493–504.
[28] D. Odstrčil, J.A. Linker, R. Lionello, Z. Mikic, P. Riley, V.J. Pizzo, and J.G. Luhmann, *Merging of coronal and heliospheric numerical two-dimensional MHD models*, J. Geophys. Res. 107 (2002), doi: 101029/1998JA900038.
[29] P. Riley, J.A. Linker, Z. Mikic, D. Odstrčil, V.J. Pizzo, and D.F. Webb, *Evidence of post-eruption reconnection associated with coronal mass ejections in the solar wind*, J. Geophys. Res. 578 (2002), pp. 972–978.
[30] M. Vandas, S. Fischer, M. Dryer, Z. Smith, and T. Detman, *Simulation of magnetic cloud propagation in the inner heliosphere in two-dimensions. 1: a loop perpendicular to the ecliptic plane*, J. Geophys. Res. 100 (1995), pp. 12,285–12,292.
[31] C.P.T. Groth, D.L. De Zeeuw, T.I. Gombosi, and K.G. Powell, *Global three-dimensional MHD simulation of a space weather event: CME formation, interplanetary propagation, and interaction with the magnetosphere*, J. Geophys. Res. 105 (2000), pp. 25,053–25,078.
[32] M. Vandas, D. Odstrčil, and S. Watari, *Three-dimensional MHD simulation of a loop-like magnetic cloud in the solar wind*, J. Geophys. Res. 107 (2002). doi: 101029/2001JA005068.
[33] P.J. Cargill, J. Schmidt, D.S. Spicer, and S.T. Zalesak, *Magnetic structure of over-expanding coronal mass ejections: numerical models*, J. Geophys. Res. 105 (2000), pp. 7509–7520.
[34] P.J. Cargill, *On the aerodynamic drag force acting on interplanetary coronal mass ejections*, Sol. Phys. 221 (2004), pp. 135–149.
[35] P. Riley and J.T. Gosling, *Do coronal mass ejections implode in the solar wind?*, Geophys. Res. Lett. 25 (1998), pp. 1529–1532.
[36] S.E. Gibson, Y. Fan, C. Mandrini, G. Fisher, and P. Demoulin, *Observational consequences of a magnetic flux rope emerging into the corona*, Astrophys. J. 617 (2004), pp. 600–613.
[37] W.B. Manchester, T. Gombosi, D. De Zeeuw, and Y. Fan, *Eruption of a buoyantly emerging magnetic flux rope*, Astrophys. J. 610 (2004), pp. 588–596.
[38] J. Lin and T.G. Forbes, *Effects of reconnection on the coronal mass ejection process*, J. Geophys. Res. 105 (2000), pp. 2375–2392.
[39] V.D. Shafranov, *Plasma equilibrium in a magnetic field*, Rev. Plasma Phys. 2 (1966), pp. 103–151.
[40] B. Kliem, V.S. Titov, and T. Török, *Formation of current sheets and sigmoidal structure by the kink instability of a magnetic loop*, Astron. Astrophys. 413 (2004), pp. L23–L26.
[41] T. Török, B. Kliem, and V.S. Titov, *Ideal kink instability of a magnetic loop equilibrium*, Astron. Astrophys. 413 (2004), pp. L27–L30.
[42] J. Lin, T.G. Forbes, P.A. Isenberg, and P. Demoulin, *The effect of curvature on flux-rope models of coronal mass ejections*, Astrophys. J. 504 (1998), pp. 1006–1019.
[43] H. Ji, H. Wang, E.J. Schmahl, Y.-J. Moon, and Y. Jiang, *Observations of the failed eruption of a filament*, Astrophys. J. Lett. 595 (2003), pp. L135–L138.
[44] J.L. Leroy, V. Bommier, and S. Sahal-Brechot, *The magnetic field in the prominences of the polar crown*, Sol. Phys. 83 (1983), pp. 135–142.
[45] W.B. Manchester, T.I. Gombosi, I. Roussev, D.L. De Zeeuw, I.V. Sokolov, K.G. Powell, G. Tóth, and M. Opher, *Three-dimensional MHD simulation of a flux rope driven CME*, J. Geophys. Res. 109 (2004), pp. 1102–1119.
[46] W.B. Manchester, T.I. Gombosi, I. Roussev, A. Ridley, D.L. De Zeeuw, I.V. Sokolov, K.G. Powell, and G. Tóth, *Modelling a space weather event from the Sun to the Earth: CME generation and interplanetary propagation*, J. Geophys. Res. 109 (2004), pp. 2107–2122.
[47] P.A. Sturrock, *The role of eruption in solar flares*, Sol. Phys. 121 (1989), pp. 387–397.
[48] T. Amari, J.F. Luciani, J.J. Aly, Z. Mikic, and J. Linker, *Coronal mass ejection: initiation, magnetic helicity, and flux ropes. II. Turbulent diffusion-driven evolution*, Astrophys. J. 595 (2003), pp. 1231–1250.
[49] J.A. Linker, R. Lionello, Z. Mikić, and T. Amari, *Magnetohydrodynamic modeling of prominence formation within a helmet streamer*, J. Geophys. Res. 106 (2001), pp. 25,165–25,176.
[50] R.L. Moore, A.C. Sterling, H.S. Hudson, and J.R. Lemen, *Onset of the magnetic explosion in solar flares and coronal mass ejections*, Astrophys. J. 552 (2001), pp. 833–848.
[51] C.R. DeVore and S.K. Antiochos, *Homologous confined filament eruptions via magnetic breakout*, Astrophys. J., 680 (2008), pp. 740–756.
[52] A.A. van Ballegooijen and P.C.H. Martens, *Formation and evolution of solar prominences*, Astrophys. J. 343 (1989), pp. 971–984.
[53] B. Inhester, J. Birn, and M. Hesse, *The evolution of line-tied coronal arcades including a converging footpoint motion*, Sol. Phys. 138 (1992), pp. 257–281.
[54] J. Zhao and A.G. Kosovichev, *Helioseismic observation of the structure and dynamics of a rotating sunspot beneath the solar surface*, Astrophys. J. 591 (2003), pp. 446–453.
[55] M.D. Altschuler, R.H. Levine, M. Stix, and J. Harvey, *High resolution mapping of the magnetic field of the solar corona*, Sol. Phys. 51 (1977), pp. 345–375.
[56] I.I. Roussev, T.I. Gombosi, I.V. Sokolov, M. Velli, W. Manchester, D.L. De Zeeuw, P. Liewer, G. Tóth, and J. Luhmann, *A three-dimensional model of the solar wind incorporating solar magnetogram observations*, Astrophys. J. Lett. 595 (2003), pp. L57–L61.
[57] B.T. Welsch, G.H. Fisher, W.P. Abbett, and S. Regnier, *ILCT: recovering photospheric velocities from magnetograms by combining the induction equation with local correlation tracking*, Astrophys. J. 610 (2004), pp. 1148–1156.
[58] E. Fermi, *On the origin of the cosmic radiation*, Phys. Rev. 75 (1949), pp. 1169–1174.
[59] I.V. Sokolov, I.I. Roussev, T.I. Gombosi, M.A. Lee, J. Kóta, T.G. Forbes, W.B. Manchester, and J.I. Sakai, *A new field-line-advection model for solar particle acceleration*, Astrophys. J. Lett. 616 (2004), pp. L171–L174.
[60] I. Ugarte-Urra, H.P. Warren, and A.R. Winebarger, *The magnetic topology of coronal mass ejection sources*, Astrophys. J. 662 (2007), pp. 1293–1301.
[61] A.J. Tylka, C.M.S. Cohen, W.F. Dietrich, M.A. Lee, C.G. Maclennan, R.A. Mewaldt, C.K. Ng, and D.V. Reames, *Shock geometry, seed populations, and the origin of variable elemental composition at high energies in large gradual solar particle events*, Astrophys. J. 625 (2005), pp. 474–495.

[62] M.A. Lee, *Particle acceleration and transport at CME-driven shocks*, in *Coronal Mass Ejections*, N. Crooker, J.A. Joselyn, and J. Feynman, eds., AGU, Washington, DC, 1997, pp. 227–234.
[63] C.K. Ng, D.V. Reames, and A.J. Tylka, *Effect of proton-amplified waves on the evolution of solar energetic particle composition in gradual events*, Geophys. Res. Lett. 26 (1999), pp. 2,145–2,148.
[64] C.K. Ng, D.V. Reames, and A.J. Tylka, *Modeling shock-accelerated solar energetic particles coupled to interplanetary Alfvén waves*, Astrophys. J. 591 (2003), pp. 461–485.
[65] I.V. Sokolov, I.I. Roussev, L.A. Fisk, M.A. Lee, T.I. Gombosi, and J.I. Sakai, *Diffusive shock acceleration theory revisited*, Astrophys. J. Lett. 642 (2006), pp. L81–L84.
[66] G.P. Zank, W.K.M. Rice, and C.C. Wu, *Particle acceleration and coronal mass ejection driven shocks: a theoretical model*, J. Geophys. Res. 105 (2000), pp. 25,079–25,096.
[67] E.W. Cliver, S.W. Kahler, and D.V. Reames, *Coronal shocks and solar energetic proton events*, Astrophys. J. 605 (2004), pp. 902–910.
[68] S. Kahler, *Injection profiles of solar energetic particles as functions of coronal mass ejection heights*, Astrophys. J. 428 (1994), pp. 837–842.
[69] A.J. Tylka, D.V. Reames, and C.K. Ng, *Observations of systematic temporal evolution in elemental composition during gradual solar energetic particle events*, Geophys. Res. Lett. 26 (1999), pp. 2141–2144.
[70] D.V. Reames, *Particle acceleration at the Sun and in the heliosphere*, Space Sci. Rev. 90 (1999), pp. 413–491.
[71] A.J. Tylka, *New insights on solar energetic particles from wind and ACE*, J. Geophys. Res. 106 (2001), pp. 25,333–25,352.
[72] N. Gopalswamy, A. Lara, M.L. Kaiser, and J.-L. Bougeret, *Near-Sun and near-Earth manifestations of solar eruptions*, J. Geophys. Res. 106 (2001), pp. 25,261–25,278.
[73] O. Cohen, I.V. Sokolov, I.I. Roussev, C.N. Arge, W.B. Manchester, T.I. Gombosi, R. Frazin, H. Park, M.D. Butala, F. Kamalabadi, and M. Velli, *A semi-empirical magnetohydrodynamical model of the solar wind*, Astrophys. J. Lett. 654 (2007), pp. L163–L166.
[74] G. Li, G.P. Zank, and W.K.M. Rice, *Energetic particle acceleration and transport at coronal mass ejection-driven shocks*, J. Geophys. Res. 108 (2003), pp. 10–21.
[75] A.M. Heras, B. Sanahuja, D. Lario, Z.K. Smith, T. Detman, and M. Dryer, *Three low-energy particle events: modeling the influence of the parent interplanetary shock*, Astrophys. J. 445 (1995), pp. 497–508.
[76] D.V. Reames, C.K. Ng, and D. Berdichevsky, *Angular distributions of solar energetic particles*, Astrophys. J. 550 (2001), pp. 1064–1074.
[77] J.R. Jokipii, *Rate of energy gain and maximum energy in diffusive shock acceleration*, Astrophys. J. 313 (1987), pp. 842–846.
[78] G.M. Webb, G.P. Zank, C.M. Ko, and D.J. Donohue, *Multidimensional Green's functions and the statistics of diffusive shock acceleration*, Astrophys. J. 453 (1995), p. 178.
[79] H. Lin, M.J. Penn, and J.R. Kuhn, *HeI 10830 Angstrom Line Polarimetry: A New Tool to Probe the Filament Magnetic Fields*, Astrophys. J. 493 (1998), pp. 978–995.
[80] R.A. Howard, J.D. Moses, D.G. Socker, K.P. Dere, J.W. Cook, and SECCHI consortium, *Sun–Earth connection coronal and heliospheric investigation (SECCHI)*, Adv. Space Res. 29 (2002), pp. 2017–2026.